

Low Q^2 Jet Production at HERA in Next-to-Leading Order QCD

G. Kramer, B. Pötter

II. Institut für Theoretische Physik*, Universität Hamburg
Luruper Chaussee 149, D-22761 Hamburg, Germany
e-mail: kramer@mail.desy.de, poetter@mail.desy.de

Abstract

We present next-to-leading order calculations of one- and two-jet production in eP collisions at HERA for photon virtualities in the range $1 < Q^2 < 100 \text{ GeV}^2$. Soft and collinear singularities are extracted using the phase space slicing method. Numerical results are presented for HERA conditions with the Snowmass jet definition. The transition between photoproduction and deep-inelastic scattering is investigated in detail. We compare two approaches, the usual deep-inelastic theory, where the virtual photon couples only directly to quarks and antiquarks, and the photoproduction approach, where the photon couples either in the direct way or in the resolved way via the parton constituents of the virtual photon with the proton constituents. Finally we compare with recent H1 data of the dijet rate obtained for various photon virtualities Q^2 with special attention to the region, in which two jets have equal transverse momenta.

*Supported by Bundesministerium für Forschung und Technologie, Bonn, Germany, under Contract 05 7 HH 92P (0), and by EEC Program *Human Capital and Mobility* through Network *Physics at High Energy Colliders* under Contract CHRX-CT93-0357 (DG12 COMA).

1 Introduction

Recently jet production in electron-proton scattering in the transition region between photoproduction and deep-inelastic scattering (DIS) has received very much attention both from the experimental [1, 2, 3] and the theoretical [4, 5, 6, 7] side.

In the photoproduction of jets, i.e., in eP collisions at HERA for photon virtualities in the region $0 \lesssim Q^2 \lesssim Q_{max}^2$ with Q_{max}^2 being small, the photon couples either directly to a parton from the proton or through resolved processes, in which the photon transforms into partons and one of these interacts with a parton out of the proton to produce jets. The cross section for jet production is expressed as a convolution of universal parton distributions of the proton and, in the resolved case, of the photon with the hard parton-parton scattering cross section. The evolution of both parton densities with the scale μ as well as the hard parton-parton scattering cross section can be calculated in perturbative QCD as long as the scale μ of the hard subprocess, which is of the order of the transverse energy E_T of the produced jets, is large enough as compared to Λ_{QCD} and Q . For these processes the photon densities are defined for photon virtualities $Q^2 = 0$ and are constructed in such a way as to describe the wealth of data in deep-inelastic $e\gamma$ scattering or $\gamma^*\gamma$ scattering, where the photon γ^* has a large virtuality.

This approach can easily be extended to the case of jet production in eP collisions with a fixed $Q^2 \neq 0$, as long as Q^2 is small enough compared to the hard scattering scale μ^2 [4, 5, 6, 7]. For this case the parton distributions of the photon depend on x and the scale μ^2 , as in real photoproduction ($Q^2 = 0$), and in addition on the virtuality Q^2 . Several models exist for describing the μ^2 evolution of these parton distribution functions (PDF's) with changing Q^2 [4, 8, 9], but very little data from deep-inelastic $e\gamma^*$ scattering with photons γ^* of virtuality $Q^2 \neq 0$ [10] exist, where they could be tested. Experimental data from jet production in the region $Q^2 \ll \mu^2 \sim E_T^2$ could help to gain information on the Q^2 evolution of these photon structure functions. Parton densities of the virtual photon are suppressed [4, 9, 11] with increasing Q^2 and are, in the usual LO definition, assumed to vanish like $\ln(\mu^2/Q^2)$ for $Q^2 \rightarrow \mu^2$, so that in the region $Q^2 \sim \mu^2$ the direct process dominates. Therefore, in the LO framework, it depends very much on the choice of scale μ^2 in relation to E_T^2 , whether a resolved contribution is present in the region $Q^2 \geq E_T^2$. This has been observed recently in a study of the dijet rate in DIS in the region $5 < Q^2 < 100 \text{ GeV}^2$ by the H1 collaboration [3, 12]. In these measurements dijets are searched with a cone-jet algorithm with radius $R = 1$ in the virtual photon-proton center-of-mass frame. The results could be described in LO by a superposition of the usual direct component and the resolved component if the scale μ^2 was chosen equal to $\mu^2 = Q^2 + E_T^2$, so that the resolved contribution was significant also for $Q^2 > E_T^2$. Of course, for a smaller scale μ^2 , as for example $\mu^2 = E_T^2$, the resolved contribution was in fact small for the region $Q^2 \geq E_T^2$, as to be expected. In this approach the resolved contribution may be considered as a NLO correction to the direct cross section, which is evaluated in the leading-logarithm approximation. This interpretation of the H1 measurements is not very satisfactory for the following reasons. First the sum of the LO direct and resolved cross section suffers from an appreciable scale dependence.

Second in the region $Q^2 \geq E_T^2$ power like terms $\propto (Q^2/E_T^2)^n$ are more important than the logarithmic ones $\propto \ln(\mu^2/Q^2)$ which are summed by using the parton PDF's of the virtual photon. To account correctly for the power behaved terms one must include the complete NLO corrections to the leading (in α_s) direct-photon contributions. So, if one wishes to cover the whole range from $Q^2 \ll E_T^2$ to $Q^2 > E_T^2$, one must still include the resolved contribution (i.e. those involving the PDF's of the virtual photon), however, in such a way that these are matched with the NLO direct photon contributions by subtracting from the latter those terms which are already included through the PDF's of the virtual photon. Such a subtraction has been worked out in our earlier work with M. Klasen [7] by separating the collinear photon initial state singularities from the NLO corrections to the direct cross section. There we studied inclusive one- and two-jet production with virtual photons in the region $Q^2 \ll E_T^2$ by transforming to the HERA laboratory system. In this system the results were compared to the photoproduction cross sections and the unsubtracted direct-photon cross section up to NLO. The dependence of the cross section on Q^2 had been investigated for some cases up to $Q^2 = 9 \text{ GeV}^2$ (please note that in [7] we used P^2 for the variable Q^2). We found that with increasing Q^2 the sum of the NLO resolved and the NLO direct cross section, in which the terms already contained in the resolved part were subtracted, approached the unsubtracted direct photon cross section. However, some difference remained even at the highest studied Q^2 .

In this paper we want to extend this work in several directions. First we calculate the two cross sections, the resolved and the subtracted direct cross section over a larger range of Q^2 , namely $1 \leq Q^2 \leq 100 \text{ GeV}^2$, including NLO corrections for both cross sections. We compare this cross section with the unsubtracted direct cross section as a function of Q^2 . Following essentially the analysis of the dijet rate of the H1 collaboration [12] we divide the Q^2 range into seven subsequent Q^2 intervals which we specify later. In the intervals with the larger Q^2 the longitudinal cross section is not negligible anymore. Therefore this cross section had to be included in the subtracted direct as well as in the unsubtracted direct cross section. Second we present our results in the photon-proton center-of-mass system as was used in the analysis of the experimental data [3, 12]. For this purpose we had to calculate the resolved cross section, usually given in the HERA laboratory system also in the virtual photon-proton center-of-mass system.

We have calculated various inclusive one-jet cross sections either as a function of the rapidity η integrated over $E_T > E_{Tmin}$ or as a function of E_T integrated over the whole accessible η range. The dijet rate needs some extra discussion, since experimentally this rate is defined with cuts on the transverse energies of both jets. In addition to the two-jet rate, which we have calculated, applying all the experimental cuts on various kinematical variables, we have computed also the usual inclusive dijet cross section as a function of E_T with the rapidities η_1 and η_2 of the two-jets integrated out.

The outline of our work is as follows. In section 2 we describe how the direct, the subtracted direct and the resolved cross section are calculated. Furthermore we describe the input PDF's of the proton and the photon. The results for the inclusive single-jet, inclusive dijet and the two-jet rate are presented in section 3. Here we discuss also some of the subtleties concerning the definition of the dijet rate and finally we compare with the

dijet data from H1 [12]. Section 4 contains a summary and an outlook to future studies in the transition region between photoproduction and the deep inelastic collision region.

2 Inclusive Single- and Dijet Cross Sections

2.1 General Structure of Cross Sections

In order to define the general structure of the cross sections, which we want to calculate, we write for the inclusive production of two jets in electron-proton scattering

$$e(k) + P(p) \rightarrow e(k') + \text{jet}_1(E_{T_1}, \eta_1) + \text{jet}_2(E_{T_2}, \eta_2) + X \quad (1)$$

Here, k and p are the momenta of the incoming electron and proton, respectively. k' is the momentum of the outgoing electron. The two jets in the final state are characterized by their transverse momenta E_{T_i} and rapidities η_i , which are the observables also in the experiment. The four-momentum transfer of the electron is $q = k - k'$ and $Q^2 = -q^2$. The phase space of the electron is parametrized by the invariants $y = pq/pk$ and Q^2 . In the case of very small virtualities $Q^2 \ll q_0^2$, where q_0 is the energy of the virtual photon, y gives the momentum fraction of the initial electron energy k_0 , carried away by the virtual photon and $y = q_0/k_0$. However, in this work we do not use this approximation, since we will consider also the range of larger Q^2 . The total energy in the eP center-of-mass system is $\sqrt{S_H}$, where $S_H = (k + p)^2$. W denotes the energy in the virtual photon-proton (γ^*P) subsystem, $W^2 = (q + p)^2$.

The hadronic cross section $d\sigma^H$ is written as a convolution of the hard scattering cross section $d\sigma_{eb}$, where the electron interacts with the parton b originating from the proton, parametrized by the PDF of the proton $f_{b/P}(x_b)$ with x_b denoting the parton momentum fraction, so that

$$d\sigma^H(S_H) = \sum_b \int dx_b d\sigma_{eb}(x_b S_H) f_{b/P}(x_b). \quad (2)$$

The cross section $d\sigma_{eb}$ for the scattering of the electron on the parton b is related to the lepton tensor $L_{\mu\nu} = 4(k_\mu k'_\nu + k'_\mu k_\nu - kk'g_{\mu\nu})$ and the hadron tensor $H_{\mu\nu}$ in the following way

$$d\sigma_{eb} = \frac{1}{4S_H x_b} \frac{4\pi\alpha}{Q^4} L^{\mu\nu} H_{\mu\nu} d\text{PS}^{(n+1)} \quad (3)$$

The phase space can be separated easily in a part dL which depends only on the electron variables and a part $d\text{PS}^{(n)}$ which depends only on the n final state particles:

$$d\text{PS}^{(n+1)} = dL d\text{PS}^{(n)} \quad (4)$$

where

$$dL = \frac{Q^2}{16\pi^2} \frac{d\phi dy dQ^2}{Q^2} \quad (5)$$

Here ϕ is the azimuthal angle of the outgoing electron, which we integrate out with the result

$$\int \frac{d\phi}{2\pi} L^{\mu\nu} H_{\mu\nu} = \frac{1 + (1-y)^2}{2y^2} H_g + \frac{4(1-y) + 1 + (1-y)^2}{2y^2} H_L \quad (6)$$

In this formula $H_g = -g^{\mu\nu} H_{\mu\nu}$ and $H_L = \frac{4Q^2}{(S_H y)^2} p^\mu p^\nu H_{\mu\nu}$ gives the contribution proportional to the cross section for longitudinal polarized virtual photons. With H_g and H_L we define the corresponding cross sections for the scattering of unpolarized transversal and longitudinal polarized virtual photons on the parton b :

$$d\sigma_{\gamma b}^U = \frac{1}{4x_b S_H y} (H_g + H_L) d\text{PS}^{(n)} = \frac{1}{4x_b S_H y} H_U d\text{PS}^{(n)} \quad (7)$$

$$d\sigma_{\gamma b}^L = \frac{1}{2x_b S_H y} H_L d\text{PS}^{(n)} \quad (8)$$

With these common definitions we can write the eb cross section averaged over the azimuthal angle

$$d\bar{\sigma}_{eb} = \frac{\alpha}{2\pi} \left(\frac{1 + (1-y)^2}{y} d\sigma_{\gamma b}^U + \frac{2(1-y)}{y} d\sigma_{\gamma b}^L \right) \frac{dy dQ^2}{Q^2} \quad (9)$$

In the limit $Q^2 \rightarrow 0$ one obtains the familiar formula for the absorption of photons with small virtuality, where $d\sigma_{\gamma b}^L$ is neglected and the transversely unpolarized cross section $d\sigma_{\gamma b}^U$ is multiplied with the differential Weizsäcker-Williams spectrum [13]

$$\frac{df_{\gamma/e}}{dQ^2} = \frac{\alpha}{2\pi} \frac{1 + (1-y)^2}{y Q^2} \quad (10)$$

This approximation can also be used for very small virtualities $Q^2 \ll E_T^2$, as we did in our earlier work [7]. For the larger Q^2 including $Q^2 \simeq E_T^2$ the longitudinal cross section must be included. We emphasize that the above formula (9) does not involve any approximations, except that terms proportional to m_e^2 are neglected. In particular we do not use the usual collinear approximation for the virtual photon, familiar from calculations for photoproduction.

As mentioned already in the previous section we want to include also the resolved contribution. In this case the photon with moderate virtuality interacts with the proton or the parton b not only as a point-like particle, as we have assumed so far, but also via the partonic constituents of the photon. This partonic structure of the photon is described by PDF's $f_{a/\gamma}^{U,L}(x_a)$, introducing the new variable x_a which gives the momentum fraction of the parton in term of the virtual photon momentum, $p_a = x_a q$. Since we must distinguish between transversely and longitudinally polarized photons in (9), we must introduce two PDF's for the photon with label U and L. To simplify the formalism we can include the case of the direct photon interaction in the PDF's of the photon by using $f_{\gamma/\gamma}^{U,L} = \delta(1-x_a)$ in the formula below. Taking everything together, the hadronic cross section $d\bar{\sigma}_H(S_H)$ can be written as a convolution of the hard scattering cross section $d\sigma_{ab}$ for the reaction

$a + b \rightarrow \text{jet}_1 + \text{jet}_2 + X$ with the PDF's of the photon $f_{a/\gamma}^{U,L}(x_a)$ and the proton $f_{b/P}(x_b)$ in the following form

$$\frac{d\sigma_H(S_H)}{dQ^2 dy} = \sum_{a,b} \int dx_a dx_b f_{b/P}(x_b) \frac{\alpha}{2\pi Q^2} \left(\frac{1 + (1-y)^2}{y} f_{a/\gamma}^U d\sigma_{ab} + \frac{2(1-y)}{y} f_{a/\gamma}^L(x_a) d\sigma_{ab} \right) \quad (11)$$

Of course, for the direct photon interaction $f_{a/\gamma}^{U,L} d\sigma_{ab} = \delta(1-x_a) d\sigma_{\gamma b}^{U,L}$.

The phase space factor in (7) and (8) depends on the number of particles in the final states. In our case we have either two or three jets in the final state. For describing the final state in terms of the relevant variables we adopt the center-of-mass system of the virtual photon and the proton. In the case of two jets in the final state, we express the respective four-momenta p_1 and p_2 by their rapidities η_1 and η_2 and their transverse energies $E_{T_1} = E_{T_2} = E_T$ in the center-of-mass system:

$$\begin{aligned} p_1 &= E_T (\cosh \eta_1, 1, 0, \sinh \eta_1) \quad , \\ p_2 &= E_T (\cosh \eta_2, -1, 0, \sinh \eta_2) \quad . \end{aligned} \quad (12)$$

From energy-momentum conservation we obtain in the case of direct production ($x_a = 1$)

$$W = E_T (e^{-\eta_1} + e^{-\eta_2}), \quad (13)$$

$$y = \frac{W^2 + Q^2}{S_H} \quad (14)$$

and

$$x_b = 1 + \frac{2W}{W^2 + Q^2} E_T (\sinh \eta_1 + \sinh \eta_2). \quad (15)$$

Here, the rapidities are defined with respect to the proton momentum direction as positive z direction. The phase space $d\text{PS}^{(2)}$ together with $dy dx_b$ can be expressed either by E_T , η_1 and y

$$d\text{PS}^{(2)} dy dx_b = \frac{1}{4\pi} \frac{W}{W^2 + Q^2} \frac{1}{W - E_T e^{-\eta_1}} d\eta_1 E_T dE_T dy \quad (16)$$

with

$$x_b = \frac{W^2}{W^2 + Q^2} \left(\frac{Q^2}{W^2} + \frac{E_T e^{\eta_1}}{W - E_T e^{-\eta_1}} \right) \quad (17)$$

or by E_T , η_1 and η_2

$$d\text{PS}^{(2)} dy dx_b = \frac{1}{2\pi S_H} \frac{W^2}{W^2 + Q^2} d\eta_1 d\eta_2 E_T dE_T \quad (18)$$

In this case x_b is given by the formula (15). The phase space with three partons or jets in the final state is more complicated and will not be written down.

As is well known the higher order (in α_s) contributions to the direct and resolved cross sections have infrared and collinear singularities. To cancel them we use the familiar techniques. The singularities in the virtual and real contributions are regularized by

going to d dimensions. In the real contributions the singular regions are separated with the phase-space slicing method based on invariant mass slicing. This way, we have for both, the direct and the resolved cross section, a set of two-body contributions and a set of three-body contributions. Each set is completely finite, as all singularities have been canceled or absorbed into PDF's. Each part depends separately on the phase-space slicing parameter y_s . The analytic calculations are valid only for very small y_s , since terms $O(y_s)$ have been neglected in the analytic integrations. For very small y_s , the two separate pieces have no physical meaning. The y_s is just a technical parameter which must be chosen sufficiently small and serves the purpose to distinguish the phase space regions, where the integrations are done analytically, from those, where they are performed numerically. The final result must be independent of the parameter y_s . In the real corrections for the direct cross section there are final state singularities and contributions from parton initial state singularities (from the proton side). They have been calculated by Graudenz [14] in connection with NLO corrections for jet production in deep-inelastic eP scattering. Since he used the same phase-space slicing method they can be taken over together with the virtual corrections up to $O(\alpha\alpha_s^2)$. To these results, which were given only for the H_g matrix element, we added the NLO contributions to H_L , so that together with the LO contributions we have both cross sections $d\sigma_{\gamma b}^U$ and $d\sigma_{\gamma b}^L$ in (9) available up to NLO. This describes the calculation of the full cross section, which is valid for general Q^2 .

The resulting NLO corrections to the direct process become singular in the limit $Q^2 \rightarrow 0$, i.e. direct production with real photons. For $Q^2 = 0$ these photon initial state singularities are usually also evaluated with the dimensional regularization method. Then the singular contributions appear as poles in $\epsilon = (4 - d)/2$ multiplied with the splitting function $P_{q_i \leftarrow \gamma}$ [15]. These singular contributions are absorbed into PDF's $f_{a/\gamma}(x_a)$ of the real photon. For $Q^2 \neq 0$ the corresponding contributions appear as terms $\ln(s/Q^2)$, \sqrt{s} being the c.m. energy of the photon-parton subprocess. These terms are finite as long as $Q^2 \neq 0$ and can be evaluated with $d = 4$ dimensions. For small Q^2 , these terms become large, which suggests to absorb them as terms proportional to $\ln(M_\gamma^2/Q^2)$ in the PDF of the virtual photon, which is present in the resolved cross section. M_γ is the factorization scale of the virtual photon. By this absorption the PDF of the virtual photon becomes dependent on M_γ^2 , in the same way as in the real photon case, but in addition it depends also on the virtuality Q^2 . Of course, this absorption of large terms is sensible only for $Q^2 \ll M_\gamma^2$. In all other cases the direct cross section can be calculated without the subtraction and the additional resolved contribution. M_γ^2 will be of the order of E_T^2 and will be specified when we present our numerical results. But also when $Q^2 \simeq M_\gamma^2$, we can perform this subtraction. Then the subtracted term will be added again in the resolved contribution, so that the sum of the two cross sections remains unchanged. This way also the dependence of the cross section on M_γ^2 must cancel, as long as we restrict ourselves to the resolved contribution in LO only.

In addition there are also finite terms (for $Q^2 \rightarrow 0$), which may be subtracted together with the singular logarithmic terms. Concerning such terms we have the same freedom as in the case $Q^2 = 0$. In our earlier work [7], we fixed these terms in such a way so that they agree with the $\overline{\text{MS}}$ factorization in the real photon case. Of course, this has

consequences concerning the selection of the PDF of the virtual photon. The details for this subtraction of the initial state singularities can be found in [7]. The cross section with these subtractions in the NLO corrections to the direct process will be denoted the subtracted direct cross section. It is clear that this cross section alone has no physical meaning. Only with the resolved cross section added it can be compared with experimental data.

In the general formula (9) for the deep-inelastic scattering cross section, we have two contributions, the transverse ($d\sigma_{\gamma b}^U$) and the longitudinal part ($d\sigma_{\gamma b}^L$). Since only the transverse part has the initial-state collinear singularity we have performed the subtraction only in the matrix element H_g which contributes to $d\sigma_{\gamma b}^U$. Therefore we do not need $f_{a/\gamma}^L$ in (11). It is also well known that $d\sigma_{\gamma b}^L$ vanishes for $Q^2 \rightarrow 0$. The calculation of the resolved cross section including NLO corrections proceeds as for real photoproduction at $Q^2 = 0$ [16], except that the cross section is calculated also for final state variables in the virtual photon-proton center-of-mass system. The kinematic relation between initial and final state variables are similar to those for direct production except that $x_a \neq 1$ and an additional integration over x_a in (11) has to be performed.

2.2 Jet Definition

The invariant mass resolution introduced in the last subsection is not suitable to distinguish two and three jets in the final state. With the enforced small values for y_s the two-jet cross section would be negative in NLO, i.e. unphysical. Therefore we must choose a jet definition that enables us to define much broader jets. We do this in accordance with the jet definition in the experimental analysis and choose the jet definition of the Snowmass meeting [17]. According to this definition, two partons i and j are recombined if for both partons i and j the condition $R_{i,J} < R$, where $R_{i,J} = \sqrt{(\eta_i - \eta_J)^2 + (\phi_i - \phi_J)^2}$, is fulfilled. η_J and ϕ_J are the rapidity and the azimuthal angle of the combined jet, respectively, defined as

$$\begin{aligned} E_{T_J} &= E_{T_i} + E_{T_j} \\ E_{T_J} \eta_J &= E_{T_i} \eta_i + E_{T_j} \eta_j \\ E_{T_J} \phi_J &= E_{T_i} \phi_i + E_{T_j} \phi_j \end{aligned} \tag{19}$$

and R is chosen as in the experimental analysis. So, two partons are considered as two separate jets or as a single jet depending on whether they lie outside or inside the cone with radius R around the jet momentum. In NLO, the final state consists of two or three jets. The three-jet sample contains all three-body contributions, which do not fulfill the cone condition. The above jet definition is applied in the hadronic center-of-mass system as in the experimental analysis. We do not introduce any additional R_{sep} parameter, which controls the recombination of partons of two adjacent cones of radius R .

2.3 Numerical Input

For the computation of the direct and resolved components in the one- and two-jet cross sections we need the PDF's of the proton $f_{b/P}(x_b)$ and of the photon $f_{a/\gamma}^U(x_a)$ in (11) at the respective factorization scales M_P and M_γ . Since we perform the subtraction only in the transversal part of the NLO direct contribution, we only use $f_{a/\gamma}^U$ and set $f_{a/\gamma}^L = 0$ in (11). For the proton PDF's we have chosen the CTEQ4M version [18], which is a NLO parametrization with $\overline{\text{MS}}$ factorization and $\Lambda_{\overline{\text{MS}}}^{(5)} = 204 \text{ MeV}$. We include $N_f = 5$ flavours. The Λ value of the proton PDF is also used to calculate α_s from the two-loop formula at the scale μ . The factorization scales are put equal to the renormalization scale μ ($M_\gamma = M_P = \mu$), where μ will be specified later. For $f_{a/\gamma}$, the PDF of the virtual photon (we skip the upper index U in the following), we have chosen one of the parametrizations of Sjöstrand and Schuler [9]. These sets are given in parametrized form for all scales M_γ , so that they can be applied without repeating the computation of the evolution. Unfortunately, these sets are given only in LO, i.e. the boundary conditions for $Q^2 = M_\gamma^2$ and the evolution equations are in LO. In [8] PDF's for virtual photons have been constructed in LO and NLO. However, parametrizations of the M_γ evolution have not been worked out. Second, these PDF's are only for $N_f = 3$ flavours, so that the charm and bottom contributions must be added as an extra contribution, which is inconvenient for us. Therefore we have selected a SaS version which includes charm and bottom as massless flavours. As explained in the previous section, we define the subtraction of the collinear singularities for the NLO direct cross section in the $\overline{\text{MS}}$ factorization. This has the consequence that, in addition to the dominant logarithmic term, also terms (in the limit $Q^2 = 0$) are left over in the NLO corrections of the subtracted direct cross section (see [7] for further details). To be consistent we must use a parametrization of the photon PDF that is defined in the $\overline{\text{MS}}$ factorization. In [9] such PDF's in the $\overline{\text{MS}}$ scheme are given in addition to the PDF's in the DIS scheme, where the finite parts are put equal to zero. Actually, this distinction is relevant only in NLO descriptions of the photon structure function. Since numerically, however, it makes a nonnegligible difference, whether one uses DIS or $\overline{\text{MS}}$ type PDF's of the photon the authors of [9] have presented both types of PDF's. Unfortunately, the $\overline{\text{MS}}$ version of [9] is defined with the so-called universal part of the finite terms, adopted from [19]. This does not correspond to the $\overline{\text{MS}}$ subtraction as we have used it in [7]. Therefore we start with the SaS1D parametrization in [9], which is of the DIS type with no finite term in $F_2^\gamma(x, M_\gamma^2)$ and transform it with the well-known formulas to the usual $\overline{\text{MS}}$ version. These transformation formulas are, for example, written down in [7] and will not be repeated here. We remark also that the Λ value of these PDF's, which determines the evolution is somewhat smaller. In [9] the value $\Lambda_{\overline{\text{MS}}}^{(4)} = 200 \text{ MeV}$ has been adopted. In addition to the distinction DIS versus $\overline{\text{MS}}$, the authors of [9] have constructed the virtual photon PDF's in different prescriptions P_0, P'_0 etc. We have chosen the PDF in the prescription P_0 , which has the property that the PDF of the virtual photon approaches the respective parton-model expression which vanishes for $Q^2 \rightarrow M_\gamma^2$ like $\ln(M_\gamma^2/Q^2)$ for the quark distributions and faster for the gluon distribution. The heavy quarks c and b are included as massless flavours except for the

starting scale Q_0 , which is $Q_0 = 600$ MeV for the u, d, s quarks and the gluon and related to the c and b quark masses, respectively.

2.4 Numerical Tests

The separation of the two-body and three-body contributions with the slicing parameter y_s is a purely technical device already mentioned in section 2.1. The sum of the two- and three-body contributions for physical cross sections must be independent of y_s . The parameter has to be quite small to guarantee that the approximations in the analytical calculations are valid. Typically, $y_s = 10^{-3}$, forcing the two-body contributions to become negative, whereas the three-body cross sections are large and positive. We have already checked in connection with our earlier work [7] that by varying y_s between 10^{-4} and 10^{-3} the superimposed two- and three-body contributions are independent of y_s for the inclusive single- and dijet cross sections. Furthermore, we have explicitly checked that the direct one- and two-jet cross sections for virtual photons are in perfect agreement with the ones from real photoproduction given in [15, 16] by integrating the virtuality over the region of small Q^2 with $Q_{min}^2 \leq Q^2 \leq 4 \text{ GeV}^2$. In this case the main contribution to the cross section comes from the lower integration boundary, where the dependence of the matrix elements on Q^2 is small. The NLO calculations are implemented in the computer program JETVIP [20]. Several other programs for calculating jet cross sections in deep-inelastic eP scattering are available, although without considering the resolved photon component. The $eP \rightarrow n$ jets event generator MEPJET [21] is also based on the phase-space slicing method. Two other NLO programs DISANT [22] and DISASTER [23] use the subtraction method. To check our cross sections away from $Q^2 \simeq 0$, we have compared JETVIP with results obtained with DISANT and found the programs to agree within 5% for all Q^2 considered in this work.

3 Results

In this section we shall present our numerical results in the form that we show first the full direct cross section including the transversal and the longitudinal part. Second, we have calculated the subtracted direct cross section and the resolved cross section which we superimpose to give the cross section which we compare with the full direct cross section. These results are presented and discussed in the following subsections for three cases, the inclusive one-jet cross section, the inclusive two-jet cross section and the exclusive two-jet rate with three separate versions of E_T cuts. The exclusive two-jet rates will be compared with recent H1 data [12]. For the comparison with these data we have considered the Q^2 bins as shown in Tab. 1. In the experimental analysis only the bins II to VII are considered. We have added the bin I in order to have results for cross sections of rather small virtuality, where the resolved part is more important than for all other bins. The bins chosen for the two-jet analysis of H1 involve some further cuts on the scattering angle and the energy of the electron in the final state. These are taken into account in

Table 1: The seven subsequent bins of photon virtuality, Q^2 , considered in this work.

Bin number	I	II	III	IV	V	VI	VII
Q^2 -range in GeV^2	[1, 5]	[5, 11]	[11, 15]	[15, 20]	[20, 30]	[30, 50]	[50, 100]

subsection 3.3 when we compare with the experimental data. For the more theoretical comparisons we have chosen simple cuts on the variable y , which is limited to the region $0.05 < y < 0.6$.

Of some importance is the choice of the scale μ . In bin I we have $Q^2 \ll E_T^2$, since in all considered cases $E_T > E_{T_{min}} > 5 \text{ GeV}$, so that $\mu = E_T$ would be a reasonable choice. Starting from bin V, $Q^2 \geq E_{T_{min}}^2$, so that from this bin on with the choice $\mu = E_T$ the resolved cross section would disappear at the minimal E_T and above up to $E_T^2 = Q^2$. In order to have a smooth behaviour for all E_T we have chosen $\mu^2 = Q^2 + E_T^2$, so that always $\mu^2/Q^2 > 1$ and in all bins a resolved cross section is generated. Of course, in the sum of the resolved and the subtracted direct cross section this scale dependence, which originates from the factorization scale dependence at the photon leg cancels to a very large extent in the summed cross section. Only the NLO corrections to the resolved cross section do not participate in the cancellation [7, 24].

3.1 Inclusive One-Jet Cross Sections

In this section, we present some characteristic results for the one-jet cross section as a function of Q^2 . For this purpose we show four selected bins I, II, V and VII, although for comparison we generated results for all seven bins, but showing them all would lead to too many figures. First, we show the rapidity distributions

$$\frac{d\sigma^{1jet}}{d\eta} = \int dE_T \frac{d^2\sigma^{1jet}}{dE_T d\eta} \quad , \quad (20)$$

where we have integrated the differential cross section over $E_T \geq 5 \text{ GeV}$. The distributions for the four Q^2 bins are presented in Figs. 1 a, b, c and d.

In the four plots we show five curves for $d\sigma/d\eta$ as a function of η in the range $-3 < \eta < 0$, since the cross section is significantly large only in the backward direction $\eta < 0$. η is the rapidity in the hadronic center-of-mass system. The five curves present the resolved cross sections (denoted by RES) in LO and NLO, the subtracted direct cross denoted DIRS, the sum of DIRS and the NLO resolved cross section, denoted SUM in the figures, and the unsubtracted direct cross section labeled DIR. This cross section should be compared to the cross section, labeled SUM (upper full curve). Both cross sections have its maximum near $\eta \simeq -2.5$. With increasing Q^2 the DIR cross section shifts its maximum to the right, whereas the summed cross section has its maximum shifted to more negative η 's. As we can see, for all four Q^2 bins the DIR cross section is always smaller than the cross

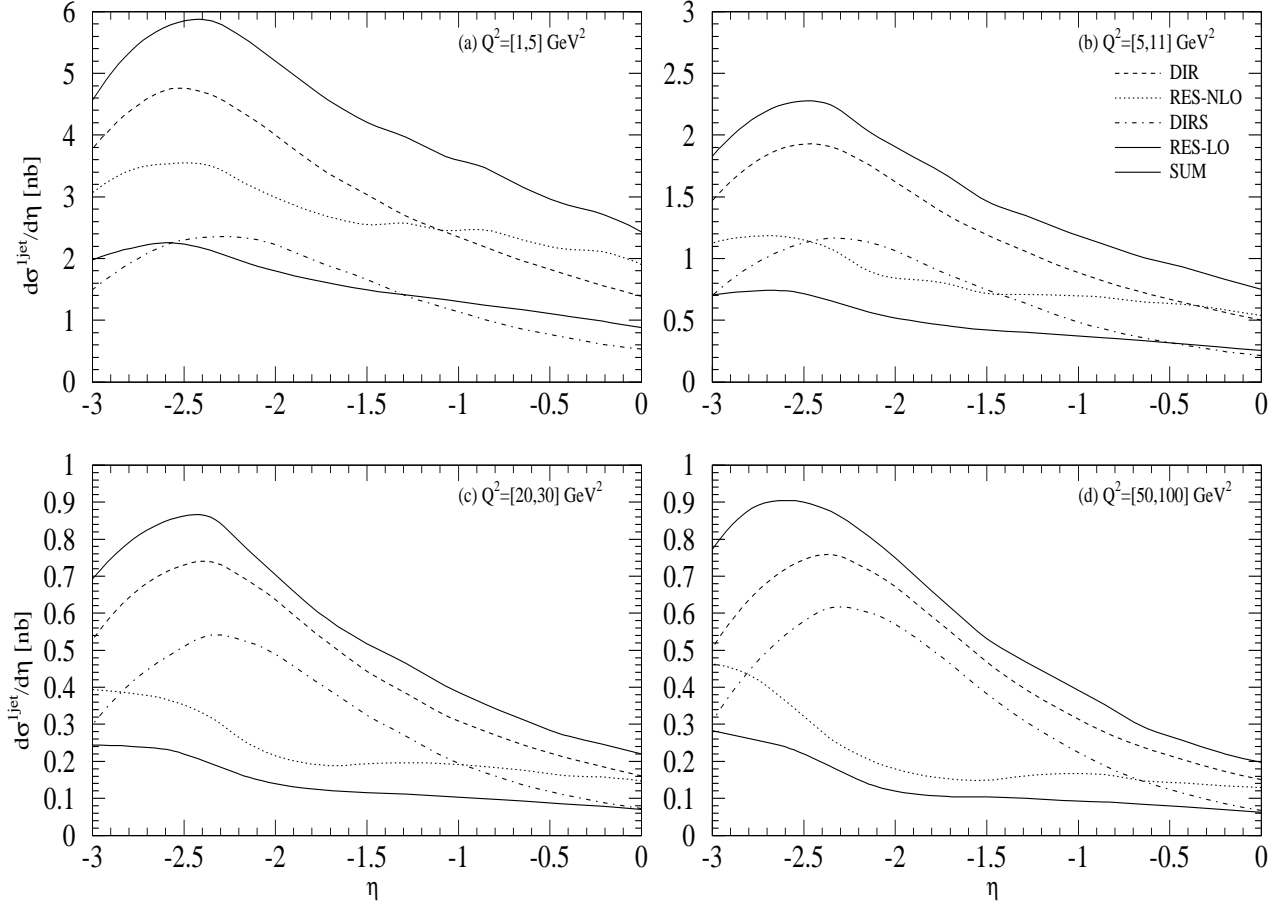


Figure 1: Inclusive single-jet cross section $d\sigma^{1jet}/d\eta$ integrated over $E_T > 5$ GeV as a function of η . In (a): $1 < Q^2 < 5$ GeV²; in (b): $5 < Q^2 < 11$ GeV²; in (c): $20 < Q^2 < 30$ GeV²; in (d): $50 < Q^2 < 100$ GeV². DIR stands for the NLO direct, DIRS is the NLO subtracted direct and RES-LO and RES-NLO are the LO and NLO resolved contributions, the lower full curve is always RES-LO, the upper one is SUM.

section obtained from the sum of DIRS and the NLO resolved cross section. Near the maximum of the cross sections they differ by approximately 25% in bin I and by 20% in the other bins. This means, at the respective Q^2 characterizing these bins, the summed cross section is always larger than the pure direct cross section. This difference originates essentially from the NLO corrections to the resolved cross section, as is obvious when we add the LO resolved curve to the DIRS contribution in Figs. 1 a, b, c and d. If we study this in more detail, we see that the sum of the LO resolved (lower full curve) and the subtracted direct cross section is somewhat below the DIR curve for $\eta < -2$ and above for $\eta > -2$ in case of bin I, below the DIR curve for all $\eta < 0$ in bin II, only slightly below the DIR curve in bin V and above the DIR curve for $\eta < -1$ and below for $\eta > -1$ in bin VII. In the largest Q^2 bin the difference is approximately 5 % near the maximum of the two curves. Near $\eta \simeq -3$ the difference is larger since the LO resolved cross section

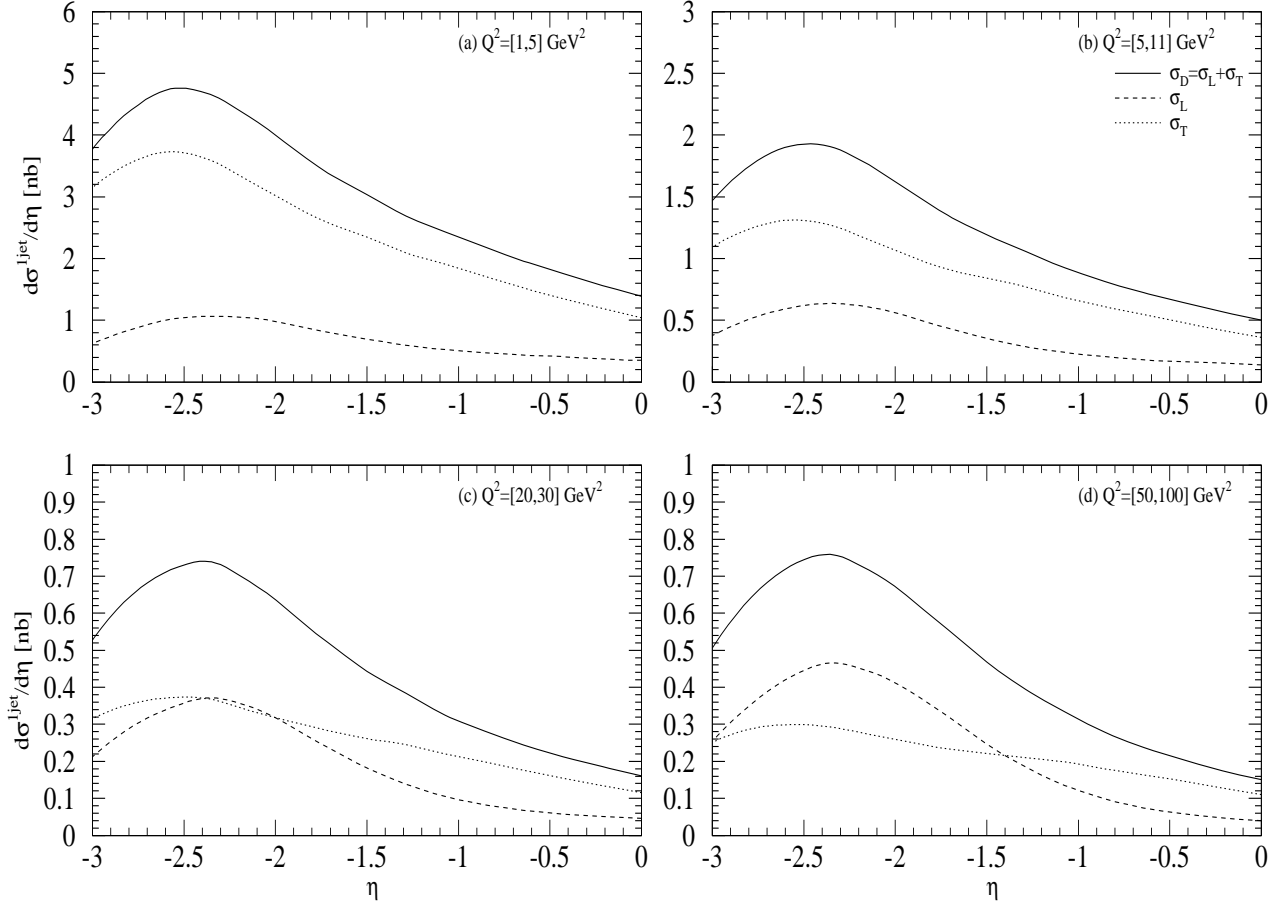


Figure 2: Transverse and longitudinal parts of the direct part of the direct inclusive single-jet cross section $d\sigma^{1jet}/d\eta$ integrated over $E_T > 5$ GeV as a function of η , for the Q^2 bins (a)–(d) as in Fig. 1. σ_T (dotted), σ_L (dashed), $\sigma_T + \sigma_L$ (full).

increases stronger towards smaller η 's than the DIRS cross section decreases. So, up to a few percent the full DIR cross section and the LO resolved plus subtracted direct cross section are equal. This means that the term subtracted in the direct cross section is replaced to a very large extent by the LO resolved cross section. Differences between these two stem from the evolution of the subtraction term to the scale $\mu = \sqrt{Q^2 + E_T^2}$. This might explain a somewhat larger difference in bin VII as compared to bin IV (not shown) and bin V. The approximate agreement between the DIR and the superimposed LO resolved and subtracted direct cross section is expected. At the considered values of $Q^2 > 1$ GeV² the virtual photon PDF is essentially given by the anomalous (or point-like) part [7]. All other contributions are of minor importance. Obviously the compensation of the LO resolved by the subtraction term is only possible, if the photon PDF is chosen consistently with the $\overline{\text{MS}}$ subtraction scheme, which is the case in our analysis. Another reason for the agreement of the NLO DIR with the sum of the subtracted direct and the LO resolved cross sections is that all contributions are of the same order in α_s , i.e. of

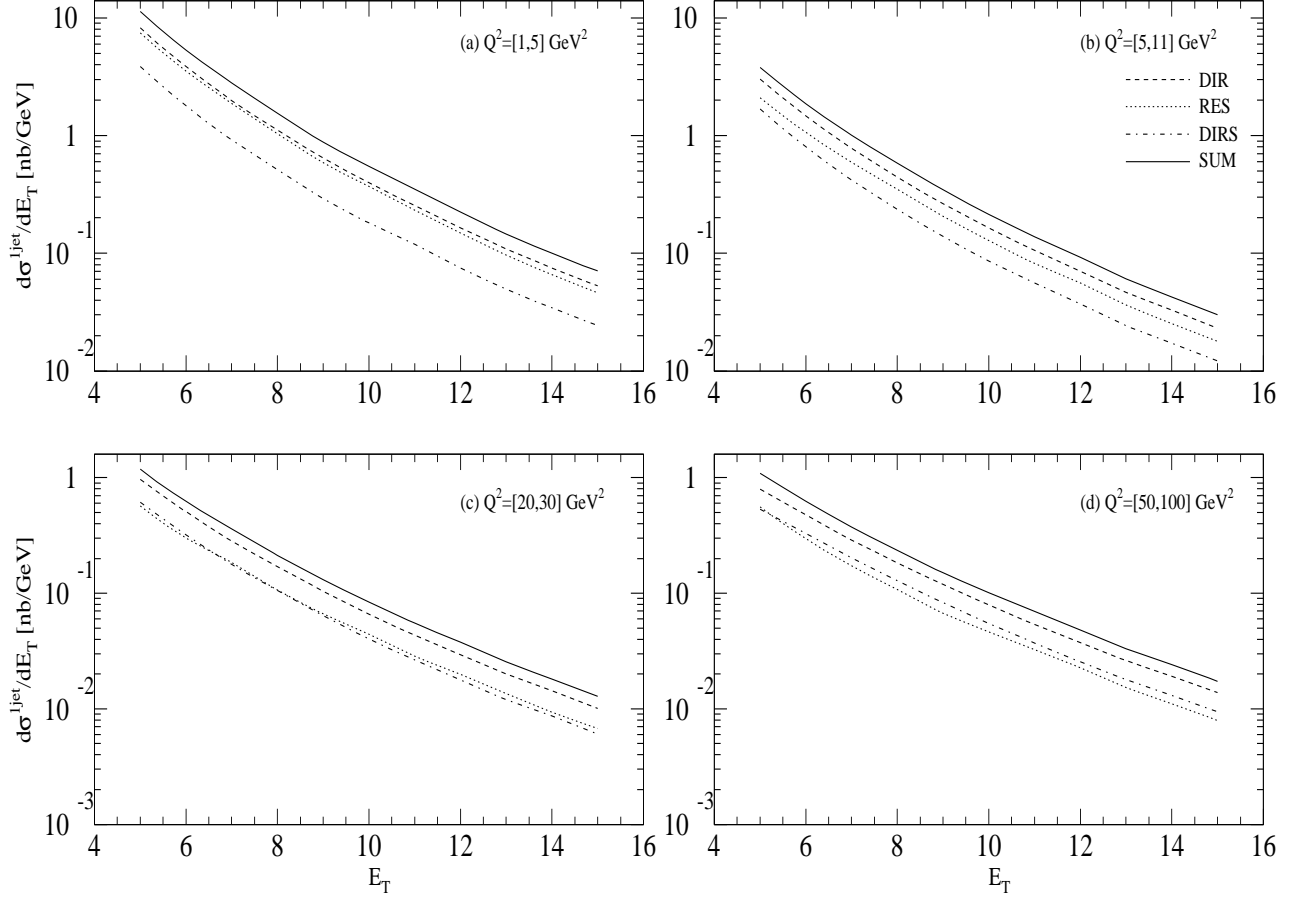


Figure 3: Inclusive single-jet cross section $d\sigma^{1jet}/dE_T$ integrated over η as a function of the transverse momentum E_T , for the Q^2 bins (a)–(d) and labeling of curves as in Fig. 1.

$\mathcal{O}(\alpha_s^2)$. This also explains that the inclusion of the NLO corrections to the resolved cross section brings in additional terms and that the sum of DIRS and the NLO resolved part lies above the pure direct cross section. We conclude that except for the lowest two Q^2 bins, the NLO direct cross section gives the same results as SUM, if we restrict ourselves to the LO contributions of the resolved cross section.

We mentioned already that in the medium Q^2 range the longitudinal cross section is not negligible. To see this more explicitly we have calculated the two contributions present in (9) separately. First we write analogous to (7) and (8) $d\sigma_{\gamma b}^U = (d\sigma_{\gamma b}^g + d\sigma_{\gamma b}^L)/2$, where $d\sigma_{\gamma b}^g$ only contains the contribution of $H_g = -g^{\mu\nu}H_{\mu\nu}$ to $d\sigma_{\gamma b}^U$. By substituting this decomposition into (9) we have calculated first the cross section $d\sigma_{eb}^T$, obtained with $d\sigma_{\gamma b}^L = 0$ in (9), i.e. just the part of the direct cross section which survives in the limit $Q^2 \rightarrow 0$, and second the cross section obtained with $d\sigma_{\gamma b}^g = 0$, i.e. the contribution which is proportional to Q^2 . For these cross sections we have integrated over $y \in [0.05, 0.6]$. These two cross sections, denoted by σ_T and σ_L are integrated over $E_T > 5 \text{ GeV}$ and calculated for all seven Q^2 bins. They are plotted as a function of η in Fig. 2 a, b, c and

d. Here we have selected the same bins as in Fig. 1, namely bin I, II, V and VII. In these figures we also show $\sigma_D = \sigma_T + \sigma_L$, which must agree with the DIR cross section in Fig. 1 a, b, c and d. We see that σ_L is small compared to σ_T in the first two bins, but still non-negligible. With increasing Q^2 the cross section σ_L increases and it is comparable to σ_T near the maximum of the cross section in bin V. In the last bin σ_L even dominates over σ_T below $\eta = -1.5$. This shows that the longitudinal part σ_L must be taken into account for $Q^2 > 1 \text{ GeV}^2$. We emphasize that the σ_L plotted in Fig. 2 includes the NLO corrections. In our earlier work [7] we have considered only σ_T , which is justified in the region $Q^2 < 1 \text{ GeV}^2$. We observe in Fig. 2 a, b, c and d, that σ_T and σ_L have a different behaviour as a function of η . σ_T is flatter, i.e. σ_L decreases much faster towards $\eta = 0$.

Next we considered the different components to the E_T distribution

$$\frac{d\sigma^{1jet}}{dE_T} = \int d\eta \frac{d^2\sigma^{1jet}}{dE_T d\eta} \quad (21)$$

of the inclusive one-jet cross section. Here we integrated over the kinematically allowed η range. The results of this cross section for the bins I, II, V and VII are shown in Fig. 3 a, b, c and d. The four cross sections DIR, DIRS, NLO resolved cross section (RES) and the sum of DIRS and the resolved cross section (SUM) are plotted. We observe in these figures a similar pattern as in the η distributions in Fig. 1 a, b, c and d. The cross section SUM is always larger than the NLO direct cross section DIR in all seven bins. The difference is approximately 30% and originates from the NLO corrections to the resolved cross section. The relation of the resolved cross section to the subtracted direct cross section DIRS changes drastically with increasing Q^2 . Whereas in the first bin (Fig. 3 a) the NLO resolved cross section is much larger than the DIRS cross section (this is similar as in photoproduction where $Q^2 = 0$), the resolved cross section is smaller than DIRS in bin VII, in particular at larger E_T . But at this larger Q^2 bin the resolved cross section is still essential and can not be neglected, compared to DIRS.

3.2 Inclusive Two-Jet Cross Sections

We now present results for the inclusive dijet cross section. The differential cross section $d^3\sigma/dE_T d\eta_1 d\eta_2$ yields the maximum of information possible on the parton distributions and is better suited to constrain them than with measurements of inclusive single jets. Since dijet production is a more exclusive process than one-jet production, the cross sections are smaller.

The selection of the variables E_T, η_1, η_2 is as for the dijet cross section in photoproduction, except that we work now in the virtual photon-proton center-of-mass system and not in the HERA laboratory system as in our previous work [7]. The variable E_T is defined to be the transverse energy of the measured (or trigger) jet, which has rapidity η_1 . The second rapidity η_2 is associated with the second jet such that in the three-jet sample these two measured jets have the largest E_T , i.e. $E_{T_1}, E_{T_2} > E_{T_3}$. A subtlety arises since at leading order the transverse energies of the two observed jets balance ($E_{T_1} = E_{T_2} = E_T$). In the three-parton events present at next-to-leading order this equality is approached in

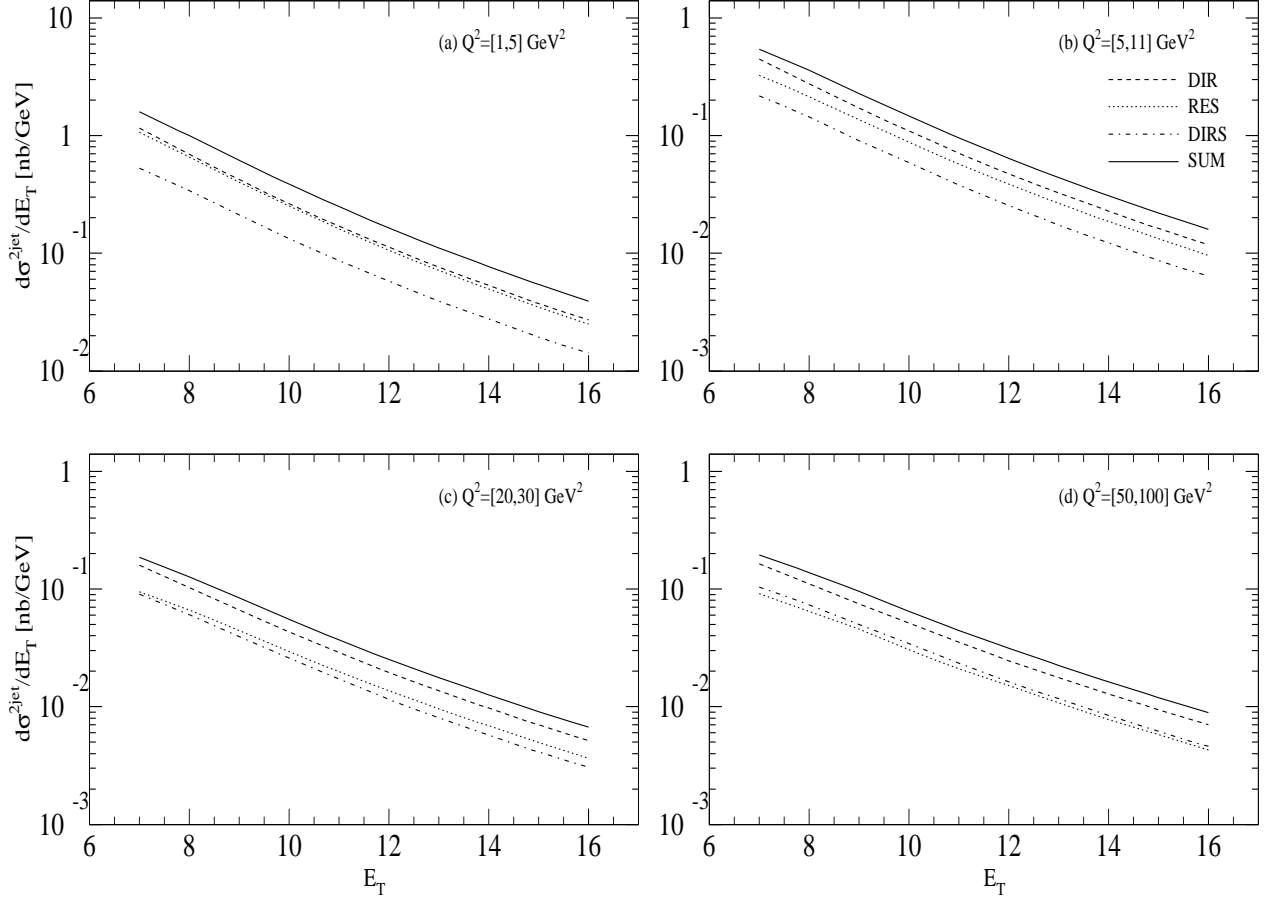


Figure 4 (a)-(d): Inclusive dijet cross section $d\sigma^{2jet}/dE_T$ integrated over the kinematically possible η_1 – and η_2 – range as a function of the transverse momentum E_T , for the Q^2 bins (a)–(d) and labeling of curves as in Fig. 1. RES is NLO resolved.

events containing two large E_T jets while the third jet has $E_{T_3} = 0$. To obtain an infrared safe cross section the E_T of the third jet must vary away from $E_{T_3} = 0$. Therefore the region $E_{T_1} = E_{T_2}$ can not be fixed and the trigger E_T assigned above can not be defined as the jet with the largest E_T . We shall come back to this point when we consider the dijet rate as measured by H1 [12].

Similar to the inclusive single-jet cross section we could predict distributions in η_1 and η_2 for fixed E_T or distributions in E_T for various values or intervals of the two rapidities η_1 and η_2 in the same way as was done for $Q^2 = 0$ [15, 16]. Since such detailed information is not expected from experiment in the near future we calculated only the distribution with the two rapidities η_1 and η_2 integrated over the kinematically allowed region. Concerning the variation with Q^2 we have done the computation again for the seven Q^2 bins defined at the beginning of this section, but we present results only for the bins I, II, V and VII. These dijet cross sections $d\sigma/dE_T$ for the four Q^2 bins are plotted in Fig. 4 a, b, c and d. We show again the full direct cross section (DIR), the NLO resolved cross section (RES),

the subtracted direct cross section (DIRS) and the sum of the latter two (SUM). The pattern of these cross sections as a function of E_T is similar as we have obtained it in Fig. 3 a, b, c and d for the one-jet cross section. The sum of NLO resolved and DIRS is always larger than the DIR cross section. The difference is again approximately 30% almost independent of Q^2 and E_T . We remark that all the components which we plotted have the same dependence and differ only in the normalization. Furthermore, similar as for the one-jet cross sections shown in Fig. 3 a, b, c and d the cross section SUM is dominated by the NLO resolved cross section in the first Q^2 bin (see Fig. 4 a) whereas the NLO resolved component and the DIRS component contribute almost equally in the last Q^2 bin. We emphasize that the sum of NLO resolved and DIRS cross section is still larger than the DIR cross section even in the highest Q^2 bin. Of course, this difference should gradually diminish with larger Q^2 , since then $\mu^2/Q^2 \rightarrow 1$ and the PDF of the virtual photon approaches zero. For the Q^2 bins considered here the difference with the DIR prediction is a NLO effect, as we have checked explicitly. This has some bearing on the determination of the strong coupling constant α_s from the inclusive single- and dijet cross sections in the Q^2 range considered in this work.

3.3 Dijet Rate and Comparison with H1 Data

In [3] preliminary data for the dijet rate R_2 as a function of Q^2 have been reported. R_2 measures the cross section for two-jet production normalized to the total eP scattering cross section in the respective Q^2 bin. The data were obtained in the bins II to VII by requiring for both jets $E_T > 5 \text{ GeV}$ in the hadronic center-of-mass frame with the additional constraints $y > 0.05$, $k'_0 > 11 \text{ GeV}$ (k'_0 is the final state electron energy), $156^\circ < \theta_e < 173^\circ$ and integrated over η_1 and η_2 with $\Delta\eta = |\eta_1 - \eta_2| < 2$. Compared to the Q^2 bins considered in the previous sections, the H1 Q^2 bins are reduced through the additional constraints on k'_0 and the electron scattering angle θ_e . In particular the bin II is reduced appreciably through these cuts. In the H1 analysis the two jets are searched for with the usual cone algorithm with $R = 1$ applied to the hadronic final state. In addition R_2 measures the exclusive two-jet rate, i.e. the contributions of more than two jets are not counted (here we discard remnant jets). As we already mentioned in the last subsection the experimental cuts $E_{T_1}, E_{T_2} \geq 5 \text{ GeV}$ are problematic from the theoretical viewpoint since the so defined cross section is infrared sensitive. With this same cut on the transverse energy of both jets there remains no transverse energy of the third jet, so that there is very little or no contribution from the three-body processes. Through the phase space slicing, needed to cancel infrared and collinear singularities in NLO, 3-body processes are always included inside the cutoff y_s , which, however, are counted in the $E_{T_1} = E_{T_2}$ contribution. For these contributions the y_s cut acts as a physical cut. In order to avoid this sensitivity on y_s one needs constraints on E_{T_1}, E_{T_2} or E_{T_3} which avoids the problematic region $E_{T_1} = E_{T_2}$. This problem was encountered already two years ago in the calculation of the inclusive two-jet cross section in photon-proton collisions [25]. The comparison with data from ZEUS required the handling of a lower E_T cut on both jets in the HERA laboratory system. To avoid the cutoff (y_s) dependence it was suggested in

[25] to arrange the two- and three-jet contributions in such a way that contributions with $E_{T_3} < 1$ GeV are included in the two-jet cross section and the contribution with $E_{T_3} > 1$ GeV in the three-jet cross section. With this additional constraint on the three-jet part one can demand $E_{T_1}, E_{T_2} > 5$ GeV. Unfortunately the constraint on E_{T_3} is very difficult to realize experimentally, because transverse energies of such low value for E_{T_3} can not be measured with sufficient accuracy. Furthermore, it is clear that in the experimental analysis the constraint $E_{T_1}, E_{T_2} > 5$ GeV is satisfied only inside some measurement errors on the transverse energies, which are not very well known, so that the constraints on E_{T_1} and E_{T_2} are not exact. Last, uncontrolled hadronization effects produce shifts between the measured jet energies and the jet energies defined in our NLO analysis.

Another possibility to remove the infrared sensitivity is to require different lower limits on E_{T_1} and E_{T_2} , as for example, $E_{T_1} > 7$ GeV, $E_{T_2} > 5$ GeV, if $E_{T_1} > E_{T_2}$ or E_{T_1} and E_{T_2} interchanged if $E_{T_2} > E_{T_1}$. This possibility was also considered in [25] in connection with the photoproduction of two jets. Then, the third jet can have enough transverse energy to avoid the infrared sensitivity. Of course, the size of the dijet cross section depends on the way the cuts on E_{T_1} and E_{T_2} are introduced. Therefore, it is important, that the same cuts are applied in the theoretical calculation and in the experimental analysis.

In the following we shall consider three possibilities for defining the two-jet rate R_2 :

- (i) Δ mode: $E_{T_1}, E_{T_2} > 5$ GeV, and if $E_{T_1} > E_{T_2}$ ($E_{T_2} > E_{T_1}$) then $E_{T_1} > 7$ GeV ($E_{T_2} > 7$ GeV)
- (ii) Σ mode: $E_{T_1}, E_{T_2} > 5$ GeV together with $E_{T_1} + E_{T_2} > 13$ GeV
- (iii) E_{T_3} mode: $E_{T_1}, E_{T_2} > 5$ GeV with the additional cut on E_{T_3} , so that contributions with $E_{T_3} < 1$ GeV are included in the two-jet cross section

The modes Δ and Σ have been applied also in the measurements of R_2 [12], so that for these two modes our results can be compared directly to the data. We give results also for the E_{T_3} mode, so one can see the differences resulting from the constraints on the R_2 rate. The Δ mode has been considered also recently in connection with inclusive two-jet photoproduction in the HERA system [26]. It is clear that the theoretical problems with the E_T cut on both jets appear equally in connection with NLO corrections to the direct as well as to the resolved cross section.

We start with the Δ mode. In Fig. 5 a we compare results for the direct cross section in LO (DIR-LO) and NLO (DIR-NLO) for three different scales $\mu = M/2, M, 2M$ where $M = \sqrt{Q^2 + E_{T_1}^2}$, calculated for the Q^2 bins II to VII with the additional cuts on k'_0 and θ_e mentioned above. We see that the NLO corrections are appreciable. Since the scale μ is rather low we have to expect such large K factors. On the other hand the scale variation is moderate, so that we are inclined to consider the NLO cross section as a safe prediction. In the LO cross section only the hard scattering cross sections are evaluated in LO whereas α_s and the parton distributions of the proton are as in the NLO calculation. In Fig. 5 b we compare the NLO direct cross section (DIR) with the sum (SUM) of the subtracted direct (DIRS) and the NLO resolved cross section (RES-NLO) for the six Q^2

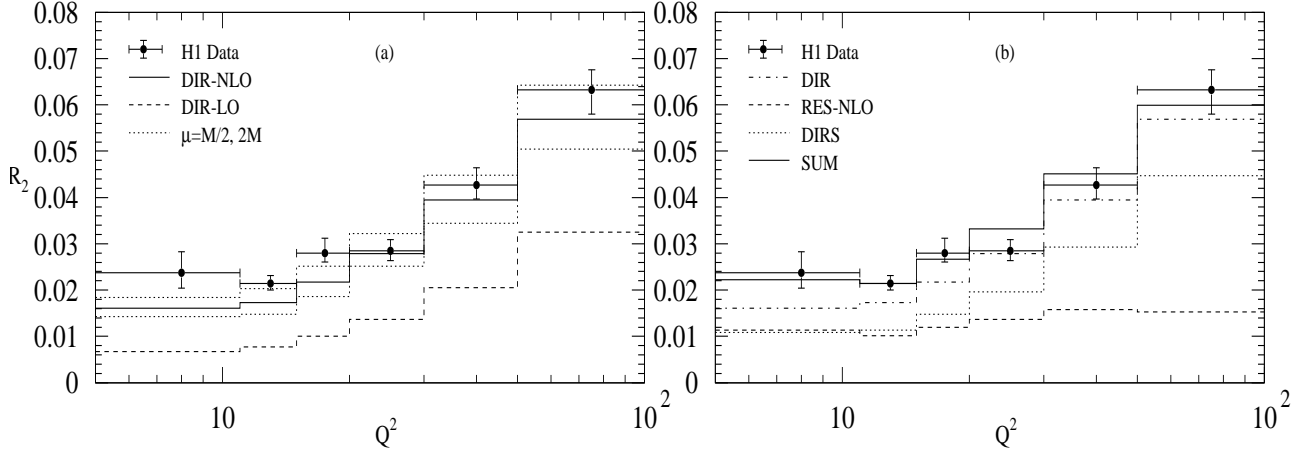


Figure 5: Dijet rate $R_2 = \sigma^{2jet}/\sigma^{tot}$ with $E_{Tmin} = 5$ GeV for the Δ mode compared to H1-data. (a) The full line corresponds to the NLO deep-inelastic dijet rate (DIR-NLO), the dashed curve gives the LO deep-inelastic dijet rate (DIR-LO). The dotted lines show the scale variation for the NLO direct, where the upper dotted curve corresponds to the smaller scale. (b) The dash-dotted curve gives the NLO direct (DIR-NLO), the dashed is NLO resolved (RES-NLO), the dotted is NLO DIRS and the full is SUM.

bins. In addition, we show the contribution of the two components (DIRS and RES-NLO) in the sum separately, similar as we have done it in the previous two subsections. In the first Q^2 bin, DIRS and the NLO resolved cross section are almost equal, the cross section in the largest Q^2 bin is dominated by DIRS. In this bin the unsubtracted direct cross section DIR is almost equal to the sum of DIRS and NLO resolved. In the first Q^2 bin this cross section is 50% larger than the NLO direct cross section. We also compare with the H1 data [12]. In the smaller Q^2 bins the sum of DIRS and NLO resolved agrees better with the experimental data than the DIR cross section. In the two largest Q^2 bins the difference of the cross sections DIR and SUM is small and it can not be decided which of these cross sections agrees better with the data due to the experimental errors. This is in contrast to the 30% difference between the DIR and SUM found for the inclusive single- and dijet cross sections which we attributed to the NLO corrections of the resolved contributions. This difference is reduced in the dijet rate R_2 due to the specific cuts on the transverse energies of the two jets in the definition of the dijet rate. These cuts suppress the resolved component stronger than the direct one, which leads to the observed behaviour of the dijet rate at the large Q^2 bins. We emphasize that the theoretical cross sections are calculated on parton level whereas the experimental two-jet rate is based on hadron jets. Corrections due to hadronization effects are estimated to be typically around 5% and at most 20% [12]. The experimental errors for R_2 consist of the combination of statistical and bin-by-bin systematic errors. An additional overall 10% systematic error connected with hadron-energy measurements is not shown and can be seen in [12].

The corresponding results in the Σ mode are plotted in Fig. 6 a and b. In Fig. 6 b

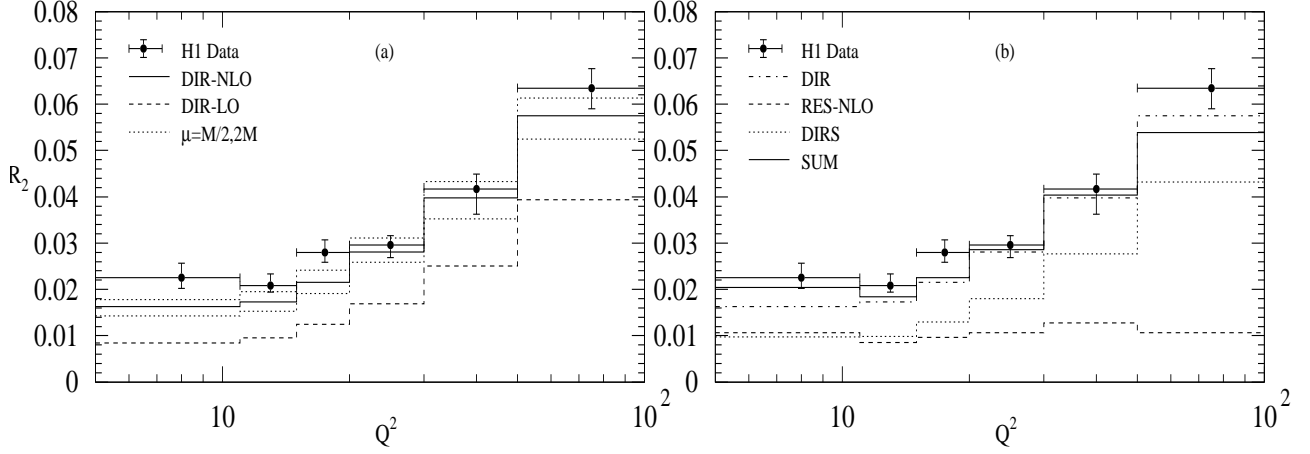


Figure 6: Dijet rate $R_2 = \sigma^{2jet}/\sigma^{tot}$ with $E_{T,min} = 5$ GeV for the Σ mode compared to H1-data. The curves in a and b are labeled as in Fig. 5.

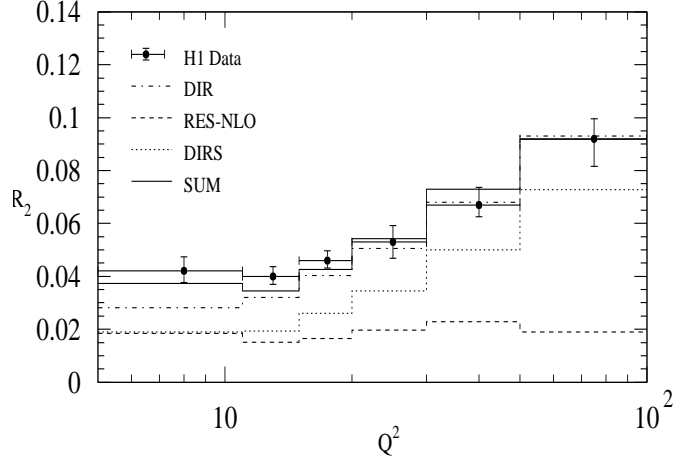


Figure 7: Dijet rate $R_2 = \sigma^{2jet}/\sigma^{tot}$ with $E_{T,min} = 5$ GeV for the E_{T_3} mode compared to H1-data. The curves are labeled as in Fig. 5 b.

we compare with the H1 data for R_2 obtained in the same mode. We observe that the theoretical results for R_2 on one side and the experimental data on the other side are very similar for the two modes. Therefore, most of the remarks made in connection with the Δ mode apply as well to the results in the Σ mode.

As the third possibility to define the exclusive two-jet rate R_2 , we consider the E_{T_3} mode with the cut $E_{T_3} < 1$ GeV. Our results for R_2 in this mode are plotted in Fig. 7, again for the four cross sections, DIR, DIRS, NLO resolved (RES-NLO) and the sum of DIRS and NLO resolved cross section (SUM). One should compare this summed cross section with the direct cross section DIR. They are more or less equal except in the first Q^2 bin, where they differ by approximately 35%. By comparing with the results in Fig. 5 b and 6 b we notice that the R_2 in the E_{T_3} mode is larger than in the other two modes. In the first Q^2 bin they differ almost by a factor of two. This shows that the way how the two-jet rate is defined theoretically or experimentally is very important. This problem

was not appreciated in the preliminary analysis [3]. In Fig. 7 we compare also with the data of H1. The agreement is very good. We note that the experimental R_2 are larger than in the modes Δ and Σ . The experimental data are obtained without any further cuts in the E_T of the two jets except $E_{T_1}, E_{T_2} > 5 \text{ GeV}$, i.e. without any E_{T_3} cut. Therefore it is not obvious that these data for R_2 correspond actually to the R_2 rate as it is defined in the theoretical calculation.

In addition to showing the exclusive two-jet cross section distributions in the trigger E_T and in the rapidities η_1 and η_2 of the two jets, as we have done it for the inclusive one-jet cross section, we discuss distributions in the ratio z , where z is defined as

$$z = -\frac{\mathbf{p}_{T_1} \cdot \mathbf{p}_{T_2}}{E_{T_1}^2} \quad (22)$$

with $E_{T_1}, E_{T_2} > E_{T_3}$ so that the jets 1 and 2 are the jets with the largest E_T . The variable z measures the imbalance in the transverse energies of these two jets. For two-body processes the two jets have balancing transverse energies and the distribution is a δ function in z , $\delta(1 - z)$. Contributions away from $z = 1$ are due to the higher order three-body contributions. The δ -function behaviour at LO is, of course, in reality modified by non-perturbative effects originating from hadronization effects and the intrinsic transverse momentum of the initial partons as well as by NLO perturbative contributions. In our calculation, none of the non-perturbative effects are taken into account. The behaviour at $z = 1$ can only be changed by NLO contributions.

In the region of z near unity one of the three partons in the three-body final state becomes soft and thus this region is sensitive to soft-gluon effects. In our calculation with an invariant mass cut slicing parameter y_s these soft-gluon corrections to the three-body processes are considered as two-body contributions as discussed in section 2. They contribute to the cross section at $z = 1$, which becomes dependent on the slicing parameter y_s in this way. To remove this dependence, i.e., to remove the infrared sensitivity, we must include a sufficiently large fraction of the genuine three-body contributions from outside $z = 1$. We do this by integrating the z distribution over a sufficiently large bin width Δz and study the exclusive two-jet cross section $d\sigma/dz$ as a function of z averaged over the bin Δz . In Fig. 8 a, b and c we display the cross sections $d\sigma/dz$ for the NLO direct, NLO resolved and the sum of the subtracted direct (DIRS) and NLO resolved cross sections. For this presentation we have included all contributions which were taken into account in the $\Delta = 2 \text{ GeV}$ mode shown in Fig. 6 a, b and c for the first Q^2 bin, i.e. we plot $d\sigma/dz$ as a function of z with $\Delta z = 0.4$ and $E_T > 5 \text{ GeV}$ and all other constraints as applied for R_2 in the Δ mode above. In Fig. 8 a the NLO direct cross section is shown. The dashed line in the region $0.8 < z < 1.2$ gives the contribution of the sum of all NLO corrections, i.e. two-body and three-body contributions. As we can see, this contribution yields already a positive cross section since the chosen bin width Δz is large enough. For a smaller bin width this contribution might be negative. The full curve in this z interval is obtained by adding the LO contribution to yield the full NLO cross section in the vicinity of $z = 1$. For $z < 0.8$ ($z > 1.2$), where the cross section receives contribution only from three-body terms, $d\sigma/dz$ decreases with decreasing (increasing) z . It is clear

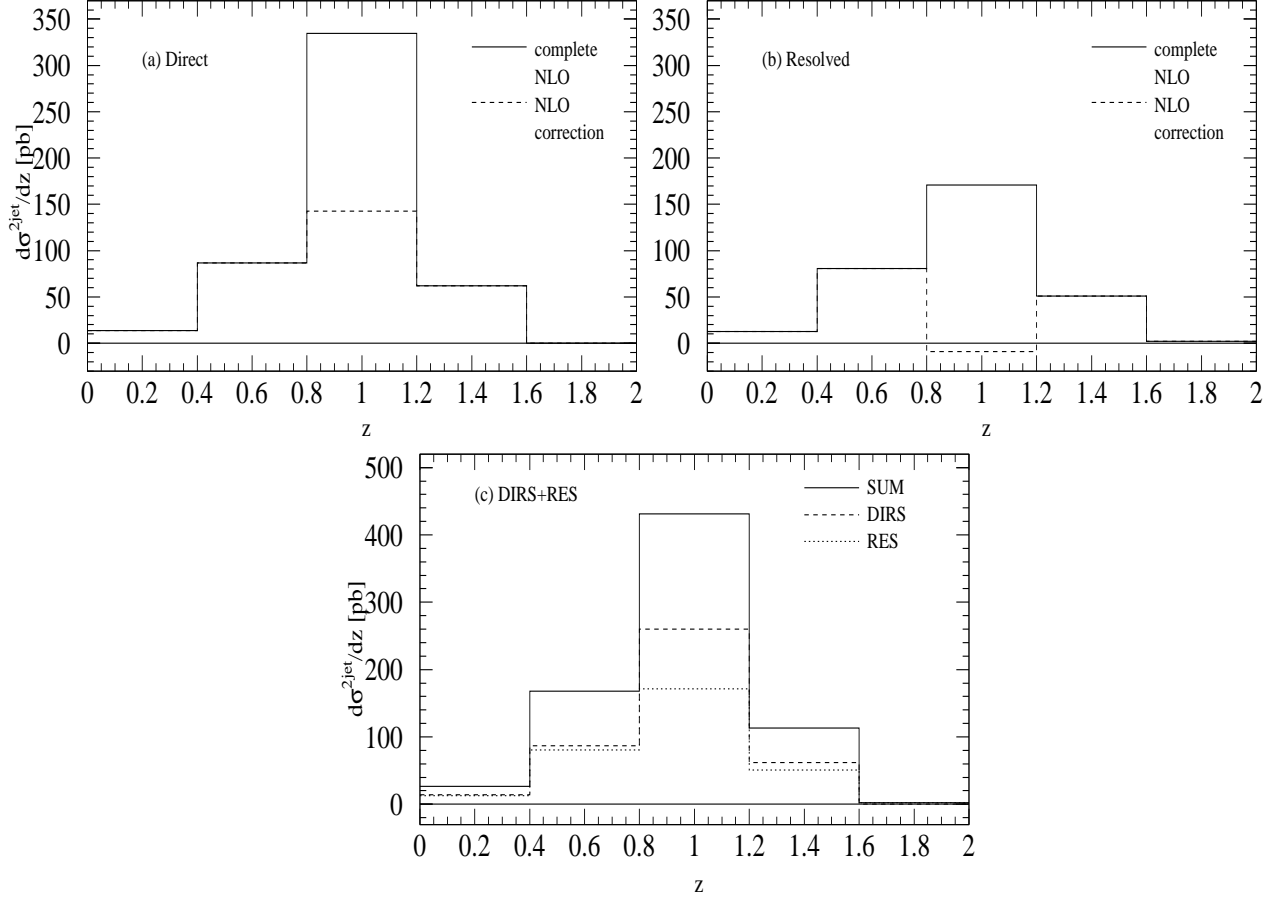


Figure 8: Dijet exclusive cross section $d\sigma^{2jet}/dz$ as a function of z in the Δ mode.
(a) Direct production: complete NLO (full curve), NLO correction (dashed curve).
(b) Resolved production: complete NLO (full curve), NLO correction (dashed curve).
(c) SUM (full), DIRS (dashed) and NLO resolved, RES (dotted).

that the cross section outside the peak at $z = 1$ is much more scale dependent than inside the peak since only three-parton terms contribute. The cross section inside the peak is a genuine NLO prediction with expected reduced scale dependence.

The resolved cross section displayed in Fig. 8 b shows a similar behaviour, except that the NLO corrections in the bin near $z = 1$ produce already a negative contribution. Since in general the NLO corrections for the resolved cross section are larger than for the direct cross section, this behaviour is to be expected. However, together with the LO term the cross section becomes positive again. In Fig. 8 c we have plotted the DIRS, the NLO resolved and their sum (SUM). This summed cross section should be compared to the complete NLO direct cross section in Fig. 8 a. For $z < 0.8$ ($z > 1.2$) the DIR and DIRS cross sections must coincide since the subtracted term contributes only to the two-body contribution. As expected from the comparison in Fig. 5 b the cross section for the sum of DIRS and NLO resolved is larger than the NLO DIR cross section. The cross sections

$d\sigma/dz$ integrated over the whole z range and divided by σ_{tot} yields the R_2 values plotted for the bin II in Fig. 5 b.

It should be mentioned that by choosing the Δ mode with $\Delta = 0$ GeV the genuine three-body contributions for $z < 0.8$ and $z > 1.2$ are reduced, since the main contribution to the dijet cross section stems from the region $E_{T_1} \simeq E_{T_2} \simeq E_{T_{min}}$, which is included in the bin around $z = 1$. Thus, not enough of the three-body contributions are available to completely remove the infrared sensitivity of the NLO calculations in the $\Delta = 0$ GeV mode. This displays in another way the need to choose experimental cuts like, e.g., in one of the modes (i)–(iii) discussed above which avoid the infrared sensitivity, if one wishes to compare NLO calculations to experimental data. In this connection it would be interesting to measure the cross section $d\sigma/dz$ as a function of the bin width Δz for one of the modes (i)–(iii). By decreasing the bin width one could investigate at which value of Δz non-perturbative and other effects come into play.

The situation with the two-jet limit $E_{T_1} = E_{T_2}$ is similar to that encountered by Aurenche et al. in connection with NLO corrections to the inclusive cross section for photon plus hadron [27] and for two-photon [28] production. Recently this problem has been discussed also by Bailey et al. [29] for the production of a prompt photon plus a charm quark in $p\bar{p}$ collisions.

4 Conclusions

We have calculated cross sections in NLO for inclusive single-jet and dijet production in low Q^2 eP scattering at HERA. The results of two approaches were compared as a function of Q^2 in the range $1 < Q^2 < 100$ GeV². In the first approach the jet production was calculated in NLO from the usual mechanism where the photon couples directly to quarks. In the second approach the logarithmic dependence on Q^2 of the NLO corrections is absorbed into the parton distribution function of the virtual photon and the jet cross sections are calculated from the subtracted direct and the NLO resolved contributions. Over the whole Q^2 range considered in this work, this sum gives on average 30% larger single-jet cross sections than the usual evaluation based only on the direct photon coupling. This difference is attributed to the NLO corrections of the resolved cross sections. If these NLO corrections are neglected the sum of the subtracted direct and the LO resolved contributions agrees with the unsubtracted direct cross sections. The additional NLO corrections to the resolved cross section will have influence on the measurement of α_s in the considered Q^2 range.

We calculated also the dijet rate based on the exclusive dijet cross section and compared it with recent H1 data. This dijet rate is plotted as a function of Q^2 , the rapidities and transverse energies are integrated with $E_T \geq 5$ GeV. The dijet rate is sensitive to the way the transverse energies of the two jets are cut. If the cuts on the E_T 's are exactly at the same value the cross section is infrared sensitive. We investigate three modes with different definitions for the kinematical constraints on the transverse energies of the measured jets. Two of them, the Δ and the Σ mode, could be realized experimentally. For

these two cases the calculated and the measured two-jet rates agree quite well over the measured Q^2 range $5 < Q^2 < 100 \text{ GeV}^2$. In the lowest Q^2 bin only the dijet rate based on the sum of the subtracted direct and resolved cross sections agrees with the experimental value. For the larger Q^2 bins the difference between the dijet rates obtained with the two approaches was small.

Future investigations of jet production in the Q^2 range considered in this work will require data on single inclusive jet production, as they exist for $Q^2 = 0$, and at larger transverse energies. This cross section does not have the problem with the lower E_T cut. With higher luminosity, a detailed dijet analysis of the triple differential cross section $d\sigma^3/dE_T d\eta_1 d\eta_2$ which is also free of the lower E_T cut problem will provide much improved information on the interplay between direct and resolved virtual photon contributions.

Acknowledgements

We are grateful to G. Grindhammer, H. Jung, H. Küster and M. Wobisch for interesting discussions on the analysis of the H1 data and for showing us their data prior to publication. We thank M. Wobisch for the calculation of the DISENT cross sections.

References

- [1] M.L. Utley on behalf of the ZEUS collaboration, Univ. Glasgow report GLAS-PPE/95-03, talk given at EPS Conference, Brussels, 1995, hep-ex/9508016; C. Foudas, ZEUS collaboration, talk given at DIS96 Workshop, Rome, 1996.
- [2] C. Adloff et al., H1 Collaboration, DESY 97-179, Phys. Lett. **B415** (1997) 418.
- [3] H. Jung, hep-ph/9709425; T. Carli, Proceedings of the Workshop 'New Trends in HERA Physics', MPI-PhE/97-22, hep-ph/9709240; D. Mikunas, 5th Int. Workshop on DIS and QCD, eds. J. Repond and D. Krakauer, Chicago (USA) 1997; M. Wobisch, same proceedings; J. Spiekermann, XXXIIInd Rencontres de Moriond, ed. J. Tran Thanh Van, Les Arces (France) 1997.
- [4] M. Glück, E. Reya, M. Stratmann, Phys. Rev. **D54** (1996) 5515.
- [5] D. de Florian, C. Garcia Canal, R. Sassot, Z. Phys. **C75** (1997) 265.
- [6] J. Chyla, J. Cvach, Proceedings of the Workshop 1995/96 on "Future Physics at HERA", eds. G. Ingelman, A. de Roeck, R. Klanner, DESY 1996, Vol. 1, p. 545.
- [7] M. Klasen, G. Kramer, B. Pötter, Eur. Phys. J. **C1** (1998) 261; B. Pötter, DESY 97-138, July 1997, hep-ph/9707319 (unpublished).
- [8] M. Glück, E. Reya, M. Stratmann, Phys. Rev. **D51** (1995) 3220.
- [9] G.A. Schuler, T. Sjöstrand, Z. Phys. **C68** (1995) 607, Phys. Lett. **B376** (1996) 193.
- [10] Ch. Berger et al., PLUTO Collaboration, Phys. Lett. **B142** (1984) 119.
- [11] F.M. Borzumati, G.A. Schuler, Z. Phys. **C58** (1993) 139.
- [12] H1 Collaboration, DESY-report in preparation; M. Wobisch, Proceedings of the 6th International Workshop on Deep Inelastic Scattering and QCD, 04–08 April 1998, Brussels.
- [13] C.F.v. Weizsäcker, Z. Phys. **88** (1934) 612; E.J. Williams, Phys. Rev. **45** (1934) 729.
- [14] D. Graudenz, Phys. Rev. **D49** (1994) 3291, Phys. Lett. **B256** (1992) 518, report DESY-T-90-01, September 1990, unpublished.
- [15] M. Klasen, G. Kramer, Z. Phys. **C72** (1996) 107.
- [16] M. Klasen, G. Kramer, Z. Phys. **C76** (1997) 489; M. Klasen, report DESY 96-204, September 1996 (unpublished); M. Klasen, T. Kleinwort, G. Kramer, report DESY 97-234, ANL-HEP-PR-97-97 December 1997.

- [17] J.E. Huth et al., Proc. of the 1990 DPF Summer Study on High Energy Physics, Snowmass, Colorado, edited by E.L. Berger, World Scientific, Singapore, 1992, p. 134.
- [18] H.L. Lai, J. Huston, S. Kuhlmann, F. Olness, J. Owens, D. Soper, W.K. Tung, H. Weerts, Phys. Rev. **D55** (1997) 1280.
- [19] P. Aurenche, M. Fontannaz, J.-Ph. Guillet, Z. Phys. **C64** (1994) 621.
- [20] B. Pötter, Proceedings of the 6th International Workshop on Deep Inelastic Scattering and QCD, 04–08 April 1998, Brussels.
- [21] E. Mirkes, D. Zeppenfeld, Phys. Lett. **B380** (1996) 23; Acta Phys. Polon. **B27** (1996) 1392.
- [22] S. Catani, M.H. Seymour, Phys. Lett. **B378** (1996) 287; Nucl. Phys. **B485** (1997) 291.
- [23] D. Graudenz, Proceedings of the Workshop 'New Trends in HERA Physics', PSI-PR-97-20, hep-ph/9709240.
- [24] D. Bödeker, G. Kramer, S.G. Salesch, Z. Phys. **C63** (1994) 471.
- [25] M. Klasen, G. Kramer, Phys. Lett. **B366** (1996) 385.
- [26] S. Frixione, G. Ridolfi, Nucl. Phys. **B507** (1997) 315.
- [27] P. Aurenche, A. Douiri, R. Baier, M. Fontannaz, D. Schiff, Z. Phys. **C24** (1984) 309.
- [28] P. Aurenche, A. Douiri, R. Baier, M. Fontannaz, D. Schiff, Z. Phys. **C29** (1985) 459.
- [29] B. Bailey, E.L. Berger, L.E. Gordon, Phys. Rev. **D54** (1996) 1896; E.L. Berger, L.E. Gordon, Phys. Rev. **D54** (1996) 2279.